RAPID COMMUNICATIONS

PHYSICAL REVIEW A VOLUME 45, NUMBER 5 1 MARCH 1992

Dynamics of a nondegenerate cascade laser

G. J. de Valcárcel,* E. Roldán, and R. Vilaseca
Departament Interuniversitari d'Optica, Universitat de València, 46100 Burjassot, Spain
(Received 23 September 1991; revised manuscript received 2 December 1991)

A model for nondegenerate cascade laser instabilities is given. The linear stability analysis of the resonant stationary solution reveals the existence of two independent Hopf bifurcations and a codimension-2 point. The system exhibits a rich dynamic behavior with transitions to chaos through the Ruelle-Takens-Newhouse scenario.

PACS number(s): 42.55.−f, 42.60.Mi

As has been shown over the last decade, lasers represent an interesting class of nonlinear physical systems since they exhibit a variety of dynamic behaviors and allow relatively simple modeling [1].

In practically all the dynamical studies, the field mode or modes are amplified through coupling with a unique medium transition. In the present work we consider a situation in which two laser-field modes are coupled with two different transitions sharing a common level (three-level cascade scheme). A rich dynamics is to be expected in this case, since in addition to the instabilities associated with each mode, further instabilities should appear as a result of the competition and coupling between both modes through the intermediate-level population and the induced two-photon coherence. At small intermediate-level detunings this configuration corresponds to a cascade laser, whereas at large detunings it can represent a two-photon laser. In this paper we present a general model (with several usual simplifications), which is solved only in the case of the cascade laser, under restricted conditions.

Some literature has been devoted to the quantum description of the cascade laser [2(a)], but, to the best of our knowledge, no attempt has been made to describe the dynamics of this laser. In the related case of the two-photon laser, both its quantum description [2(a),2(b)] and dynamics [3] have been considered, the latter, however, through a two-level model that does not contain the cascade limit. Finally, some experiments on cascade lasers have been carried out [4], although not in the dynamic version, raising the possibility for experimental verification of the results provided by our model.

We consider a three-level active medium (levels 1, 0, and 2; see the inset of Fig. 1), and two generated electric fields, $\mathcal{E}_1$ and $\mathcal{E}_2$, inside a ring cavity [5]. If the frequencies of the dipolar transitions ($2\rightarrow 0$ and $0\rightarrow 1$) are sufficiently different, and the cavity is properly tuned, we may assume that each field is coupled with only one transition ($\mathcal{E}_1$ with the lower one and $\mathcal{E}_2$ with the upper one) (nondegenerate case). In the usual semiclassical formalism (plane wave and uniform field limits) and considering single-mode unidirectional emission, these fields can be expressed as

$$\mathcal{E}_j(z,t)=\tfrac{1}{2}\mathbf{e}_j E_j(t)\exp[-i(\omega_j t+\phi_j(t)-k_j z)]+\text{c.c.}, \quad (1)$$

($j=1,2$), where z is the propagation direction along the laser cavity, and $\mathbf{e}_j$, $E_j(t)$, k_j, ω_j, and $\phi_j(t)$ represent the polarization vector, slowly varying real field amplitude, wave number, reference frequency, and phase of the field $\mathcal{E}_j(z,t)$. The total field is $\mathcal{E}(z,t)=\mathcal{E}_1(z,t)+\mathcal{E}_2(z,t)$. Denoting by ω_{20}, ω_{01}, and ω_{21} the frequencies of the one-photon ($2\rightarrow 0$ and $0\rightarrow 1$) and two-photon ($2\rightarrow 1$) transitions, respectively, the detuning of the field $\mathcal{E}_2$ is given by $\delta=\omega_2-\omega_{20}$, and the two-photon detuning by $\epsilon=\omega_2+\omega_1-\omega_{21}$ (inset of Fig. 1). Each level j ($j=1,0,2$) is populated at a constant incoherent pumping rate λ_j, and relaxation occurs at a rate γ_j. Inhomogeneous broadening is not considered.

In the usual rotating-wave and slowly varying envelope approximations, using the semiclassical density-matrix formalism [6], the Maxwell-Schrödinger equations for the laser system are

$$\begin{aligned}
\dot\rho_{22}&=-\gamma_2\rho_{22}+\lambda_2-2\alpha_2\,\mathrm{Im}(\rho_{02}),\\
\dot\rho_{00}&=-\gamma_0\rho_{00}+\lambda_0+2\alpha_2\mathrm{Im}(\rho_{02})-2\alpha_1\,\mathrm{Im}(\rho_{10}),\\
\dot\rho_{11}&=-\gamma_1\rho_{11}+\lambda_1+2\alpha_1\,\mathrm{Im}(\rho_{10}),\\
\dot\rho_{02}&=-[\Gamma_{02}+i(\dot\phi_2+\delta)]\rho_{02}+i\alpha_2 D_2+i\alpha_1\rho_{12},\\
\dot\rho_{10}&=-[\Gamma_{10}+i(\dot\phi_1-\delta+\epsilon)]\rho_{10}+i\alpha_1 D_1-i\alpha_2\rho_{12},\\
\dot\rho_{12}&=-[\Gamma_{12}+i(\dot\phi_1+\dot\phi_2+\epsilon)]\rho_{12}-i\alpha_2\rho_{10}+i\alpha_1\rho_{02},\\
\dot\alpha_{2(1)}&=-\kappa_{2(1)}\alpha_{2(1)}+g_{2(1)}\,\mathrm{Im}(\rho_{02(10)}),\\
\dot\phi_{2(1)}&=(\omega^c_{2(1)}-\omega_{2(1)})-g_{2(1)}\,\mathrm{Re}(\rho_{02(10)})/\alpha_{2(1)},
\end{aligned} \quad (2)$$

where $\rho_{jj}(t)$ represents the (real) population of the level j, $D_2\equiv\rho_{22}-\rho_{00}$ and $D_1\equiv\rho_{00}-\rho_{11}$ are the population inversions, and $\rho_{jl}(t)$ is the slowly varying complex amplitude of the coherence associated with the transition $j\rightarrow l$ ($j,l=1,0,2$), which relaxes at a rate Γ_{jl}. $2\alpha_j$ is the Rabi frequency for the field $\mathcal{E}_j$, $\alpha_j(t)=(\boldsymbol{\mu}_{0j}\cdot\mathbf{e}_j/2\hbar)E_j(t)$, where $\boldsymbol{\mu}_{0j}$ represents the (real) electric-dipole matrix element between states $|0\rangle$ and $|j\rangle$ ($\boldsymbol{\mu}_{12}=\boldsymbol{\mu}_{jj}=\mathbf{0}$). κ_j and g_j represent the cavity losses and the gain parameter ($g_j=\omega_j\mu_{0j}^2 N/2\varepsilon_0\hbar$, being N the number of active molecules per unit volume) for the field $\mathcal{E}_j$, and ω_j^c ($j=1,2$) represents the closest empty-cavity mode frequency.

System (2) is composed of eleven coupled nonlinear real first-order differential equations, since those for $\dot\phi_1(t)$ and $\dot\phi_2(t)$ can be introduced into the remaining equations. The amplitudes ρ_{02} and ρ_{10} are proportional to the medi-

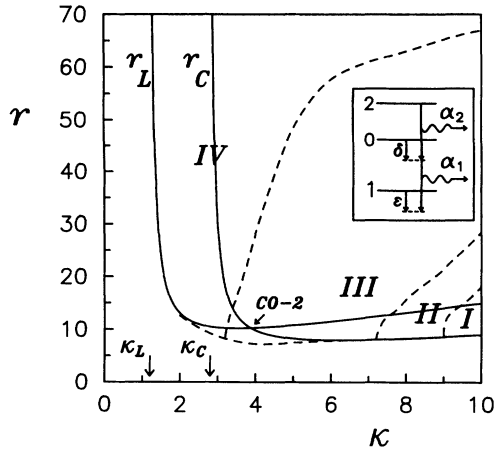

FIG. 1. Location on the κ,r plane of the Hopf bifurcations r_L and r_c (continuous lines), and the different regions of dynamic behavior I, II, III, and IV (approximately limited by the dashed lines), for $\gamma=0.2$ and $\Gamma=1.0$ (in this case, $\kappa_L=1.2$ and $\kappa_c=2.8$). For an explanation see the text. The inset shows a schematic of the cascade laser.

um polarizations at the field frequencies and ρ_{12} is responsible for the two-photon processes.

This general model properly represents a cascade laser in the limit of small δ, whereas, as mentioned above, it can represent a two-photon laser in the opposite limit ($|\delta| \gg \Gamma_{20},\Gamma_{01}$) [7]. In the following we restrict the case to that of a fully resonant cascade laser, i.e., $\delta=\epsilon=0$, choosing $\omega_j=\omega_j^c$ ($j=1,2$).

For the sake of simplicity, we will consider the particular case of identical parameters for both $2\rightarrow 0$ and $0\rightarrow 1$ transitions ($\gamma_1=\gamma_0=\gamma_2\equiv\gamma_\parallel$, $\Gamma_{10}=\Gamma_{02}\equiv\gamma_\perp$), while the constant relaxation rate for the two-photon coherence, $\Gamma_{12}\equiv\Gamma$, is allowed to be different to that of the dipoles. Under the above assumptions Eqs. (2) become the following set of seven real equations:

$$\begin{aligned}
&\dot{D}_{2(1)}=-\gamma D_{2(1)}+\bar{\lambda}_{2(1)}-4\alpha_{2(1)}y_{2(1)}+2\alpha_{1(2)}y_{1(2)}\,,\\
&\dot{y}_{2(1)}=-y_{2(1)}+\alpha_{2(1)}D_{2(1)}+(-)\alpha_{1(2)}x\,,\\
&\dot{x}=-\Gamma x+\alpha_2 y_1-\alpha_1 y_2\,,\\
&\dot{\alpha}_{1(2)}=-\kappa_{1(2)}\alpha_{1(2)}+g_{1(2)}y_{1(2)}\,,
\end{aligned}\tag{3}$$

where $y_1\equiv\mathrm{Im}(\rho_{10})$, $y_2\equiv\mathrm{Im}(\rho_{02})$, and $x\equiv\mathrm{Re}(\rho_{12})$; $\bar{\lambda}_2\equiv\lambda_2-\lambda_0$, $\bar{\lambda}_1\equiv\lambda_0-\lambda_1$. All frequencies are normalized to $\gamma_\perp$ and $\gamma\equiv\gamma_\parallel/\gamma_\perp$. The rest of the variables not appearing in Eqs. (3) are null.

The nontrivial solution (with α_1 and α_2 different from zero) of Eqs. (3) is greatly simplified if one takes $C_1=C_2\equiv C$ ($C_i\equiv g_i/\kappa_i$) [8] and $\bar{\lambda}_2=\bar{\lambda}_1$ (equal pump for both transitions), becoming

$$\begin{aligned}
&\alpha_1=\alpha_2=\pm\sqrt{\gamma(r-1)/2},\ y_{1(2)}=\alpha_{1(2)}/C\,,\\
&D_2=D_1=\frac{1}{C},\ x=0\,,
\end{aligned}\tag{4}$$

where $r=(\lambda_2-\lambda_1)C/2\gamma$ is the pump parameter. Note that (4) is a scaled version of the stationary solution of the Lorenz model [9]. $x=0$ denotes the absence of two-photon coherence in this situation.

Equations (3) also have stationary solutions other than (4) in which only one field is non-null. However, in this particular case ($\bar{\lambda}_2=\bar{\lambda}_1$, $C_2=C_1$), these solutions are always unstable.

The linear stability analysis (LSA) of solution (4) leads to a seventh-order polynomial in the eigenvalues, from which the instability thresholds cannot be derived explicitly. Nevertheless, if one further assumes $g_2=g_1$ ($\kappa_2=\kappa_1\equiv\kappa$, since $C_2=C_1$), the characteristic polynomial becomes factorized into a cubic and a fourth-order one, thus greatly simplifying this LSA. Although this last assumption is unrealistic in principle, the results we summarize next provide a qualitatively good description of situations for which $0.25\lesssim g_1/g_2=\kappa_1/\kappa_2\lesssim 4$.

The cubic part of the characteristic equation is formally identical to that obtained in the Lorenz model, giving rise to instabilities for $r>r_L\equiv\kappa(\kappa+\gamma+3)/(\kappa-\gamma-1)$ through a Hopf bifurcation if $\kappa>\kappa_L\equiv\gamma+1$ ("bad-cavity" condition) [9].

From the fourth-order polynomial we obtain an independent Hopf bifurcation at $r=r_c$ satisfying the equation

$$a(r_c-1)^2+b(r_c-1)+c=0\,,\tag{5}$$

where

$$\begin{aligned}
a&=2\gamma^2\xi(\kappa_c-\kappa)\,,\\
b&=2\gamma^2(\kappa+1)(\kappa_c-\kappa)+\gamma(\gamma+\Gamma)\xi\theta\\
&\quad-6\kappa\gamma\Gamma(\kappa+\Gamma+\gamma+1)^2\,,\\
c&=\gamma\Gamma(\kappa+1)(\gamma+\Gamma)\theta\,,
\end{aligned}\tag{6}$$

with $\kappa_c\equiv 2+(\Gamma+3\gamma)/2$, $\theta\equiv(\kappa+1)(\kappa+\Gamma+\gamma+1)+\gamma\Gamma$, and $\xi\equiv 6\kappa+3\Gamma+\gamma$. c is always positive, $a\leq 0$ for $\kappa\geq\kappa_c$, and the sign of b depends on (κ,γ,Γ). These facts condition the existence of the Hopf bifurcation at $r=r_c$ in the following way. (i) If $\kappa>\kappa_c$ only one solution exists for (5), and instabilities occur for $r\geq r_c$. (ii) If $\kappa<\kappa_c$, Eq. (5) predicts two Hopf bifurcations at $r=r_c^{\pm}$ whenever $b<0$ and $b^2>4ac$ (otherwise no solution exists for r_c); under these conditions, instabilities hold for $r_c^-\leq r\leq r_c^+$.

When both thresholds r_c and r_L exist, only the minor of them makes sense, except when $r_L>r_c^+$, in which case the three thresholds (r_c^-, r_c^+, and r_L) are meaningful since instabilities hold for $r_c^-\leq r\leq r_c^+$ or $r\geq r_L$. Notice that while r_c is Γ dependent this is not the case for r_L.

By way of example, Fig. 1 shows the location of these thresholds as a function of the cavity losses κ for the case $\gamma=0.2$ and $\Gamma=1.0$ (in this case r_c does not exist for $\kappa<\kappa_c$). Three main features can be observed: (i) Instabilities appear only for $\kappa>\kappa_L$, i.e., the "bad-cavity" condition must be fulfilled. (ii) Upon increasing r the Hopf bifurcation takes place at $r=r_L$ for a certain domain of cavity losses (between κ_L and, in the present case, $\kappa=3.873$), while above this domain the Hopf bifurcation occurs at $r=r_c$ since $r_c<r_L$. (iii) The minimum value of the threshold r_c can be smaller than that of the Lorenz model r_L [by increasing Γ, the curve r_c is lowered and shifted to the left, becoming closer to the vertical line $\kappa=\kappa_L$: in the limit $\Gamma\rightarrow\infty$—adiabatic elimination of the

two-photon coherence—$r_c^- = (r_L+2)/3 \leq \frac{11}{27} r_L$].

Feature (ii), above, is related to the crossing between the r_L and r_c curves which defines a codimension-2 point [10] ($\kappa = 3.873$, $r = 10.248$ in the case of Fig. 1). This point exists whenever r_c does. The rich dynamics expected in the neighborhood of this codimension-2 point will be the object of future work. Next we discuss the basic dynamical features of the resonant nondegenerate cascade laser.

Numerical analysis of Eqs. (3) in the dynamic domain reveals the existence of periodic and chaotic regimes. In Fig. 1 the zones of different dynamic behavior obtained by hard-mode excitation are marked with roman numerals. In region I a one-sided period-1 attractor is found [Figs. 2(a) and 2(b)]; in fact, there are two coexisting one-sided attractors, corresponding to the symmetry properties of Eqs. (3). Similar behaviors have been reported by Ning and Haken in the Lorenz model by using the anomalous switching technique [11]. In region II a chaotic two-sided attractor is found [Figs. 2(c) and 2(d)]. The closer the set of parameters is to region I the longer the trajectory remains in each lobe of the attractor before jumping to the other side. This indicates that the two-sided attractor appears as a progressive merging of the two symmetric one-sided attractors of region I. In region III a two-sided period-1 attractor is found [Figs. 2(e) and 2(f)]. Finally, in region IV, which extends to arbitrarily large values of r, chaos is again obtained [Figs. 2(g) and 2(h)]. Note the differences with respect to the chaos in region II.

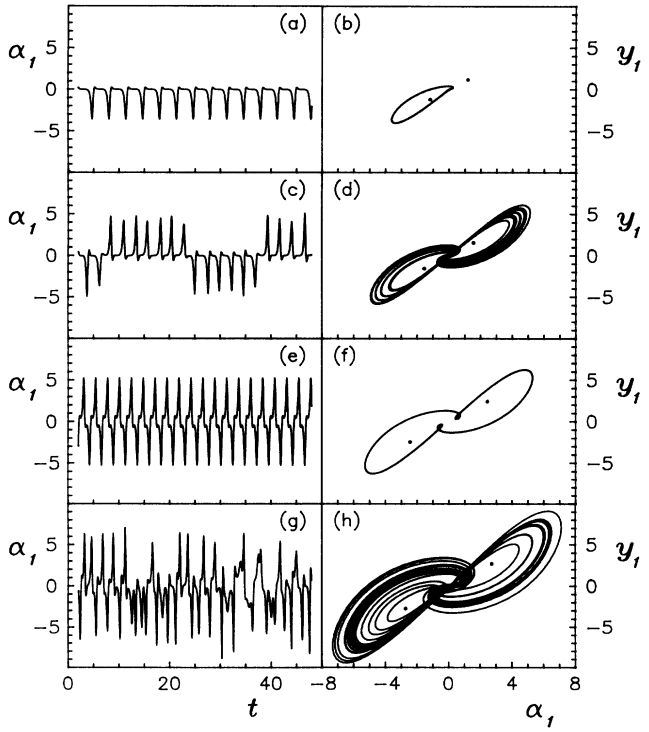

FIG. 2. Dynamic behavior of the resonant nondegenerate cascade laser for $\gamma = 0.2$, $\Gamma = 1.0$, and $\kappa = 10.0$. Left column shows the temporal evolution of field 1 and the right column shows the corresponding attractor projection on the field-polarization plane for increasing values of r [(a),(b), $r = 15.0$; (c),(d), $r = 25.0$; (e),(f), $r = 60.0$; (g),(h), $r = 75.0$]. The two points marked in (b), (d), (f), and (h) indicate the projection of the corresponding (unstable) stationary solution. All transients have been removed.

An inspection of Fig. 2 shows that a qualitative similarity exists between the attractor projections and equivalent ones in the Lorenz model [1,11]. In fact Eqs. (3), in this particular case ($\bar{\lambda}_2 = \bar{\lambda}_1$, $g_2 = g_1$, $\kappa_2 = \kappa_1$), always allow a solution $a_1(t) = a_2(t)$, $y_1(t) = y_2(t)$, $D_1(t) = D_2(t)$, $x = 0$, for which these equations are decoupled into (a_1, y_1, D_1) and (a_2, y_2, D_2), becoming isomorphic to two equal (synchronized) Lorenz models. This isomorphism applies not only to the stationary solution (4), but also to any dynamic solution of the Lorenz model. In the cascade laser, however, this dynamic solution actually represents a repeller, since it is unstable with respect to any small perturbation (e.g., any fluctuation "turns on" the variable x). From this point of view, the actual (attracting) cascade laser solutions (Fig. 2) would be expected to be different, rather than similar, to the Lorenz-type solutions. What happens is that the cascade laser solutions differ with respect to the Lorenz-type ones mostly in the "relative phase" between field intensities a_1^2 and a_2^2, which locks to half an intensity period in the cases of periodic regime (i.e., a_1^2 is maximum when a_2^2 is near zero, and vice versa), and becomes unlocked for chaotic regimes. Attractor projections on the variables associated to only one of the two fields, however, retain in some cases Lorenz-type features, since in both cases the attractive and repulsive directions remain basically the same in these projections, as a result of the mathematical similarity discussed above.

Nevertheless, there is an outstanding feature that makes the dynamics of the cascade laser different than that of the Lorenz-Haken model and most of the laser systems: In our case all the transitions from periodic orbits to chaos occur through the Ruelle-Takens-Newhouse scenario [12]. This is illustrated in Fig. 3, in which the power spectrum $S(\omega)$ of the field $a_1(t)$ is shown for three increasing values of r corresponding to crossing the border between regions III and IV in Fig. 1 for $\kappa = 10.0$. The

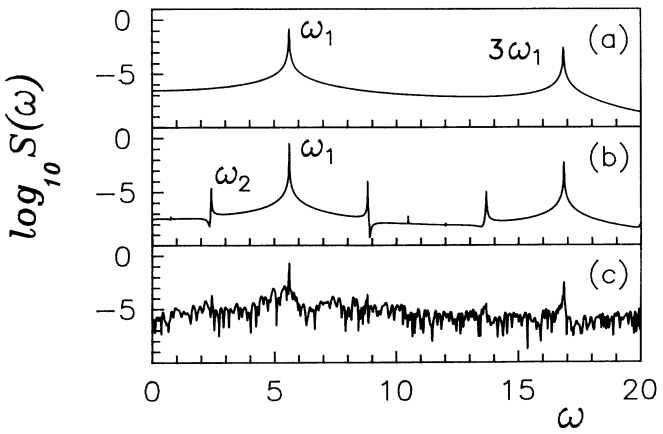

FIG. 3. Logarithm of the power spectrum $S(\omega)$ of $a_1(t)$ for pump parameters (a) $r = 66.35$, (b) $r = 66.40$, and (c) $r = 66.45$. Note the appearance of a frequency ω_2 (incommensurate with ω_1) in (b) which denotes the existence of a torus T^2. (Other parameters are as in Fig. 2.)

domain of stability of the torus T^2 [Fig. 3(b)] involved in this scenario lasts only a few hundredths of r (see figure caption). The torus T^3 possible in this route to chaos has not been found. To our knowledge this is one of the few cases [1,13] in which the Ruelle-Takens-Newhouse scenario has been found in an autonomous-laser model.

In conclusion, our analysis has provided evidence for interesting dynamical features in the cascade laser model, which should stimulate experimental verification in molecular and atomic lasers.

We acknowledge fruitful discussions with C. O. Weiss and useful information from B. Wellegehausen. This work is supported by the Dirección General de Investigación Científica y Técnica (Spain), Project No. PB89-0319-C03-03.

*Permanent address: Department de Física Aplicada, Universitat Politècnica de València, 46020-València, Spain.

[1] See, for instance, C. O. Weiss and R. Vilaseca, *Dynamics of Lasers* (VCH, Weinheim, 1991); *Instabilities and Chaos in Quantum Optics,* edited by F. T. Arecchi and R. G. Harrison (Springer-Verlag, Berlin, 1987).

[2] See, for instance, (a) A. W. Boone and S. Swain, Quantum Opt. **1**, 27 (1989); (b) Y. Zhu and X. S. Li, Phys. Rev. A **36**, 3889 (1987); Y. Zhu and M. O. Scully, *ibid.* **38**, 5433 (1988); A. W. Boone and S. Swain, Phys. Rev. A **41**, 343 (1990).

[3] C. Z. Ning and H. Haken, Z. Phys. B **77**, 157 (1989); **77**, 163 (1989).

[4] (a) H. Schlemmer, D. Fröhlich, and H. Welling, Opt. Commun. **32**, 141 (1980); (b) J. Won, Opt. Lett. **8**, 79 (1983); J. Won and G. D. Willenberg, Appl. Phys. B **31**, 5 (1983).

[5] In Ref. [4(a)] a configuration with two rings sharing a common branch (in which the amplifying medium was placed) was used. This setup has the advantage that detuning and losses for each field can be independently controlled.

[6] M. Sargent III, M. O. Scully, and W. E. Lamb, *Laser Physics* (Addison-Wesley, Reading, 1974).

[7] Two-photon amplification can be achieved through incoherent pumping [4(a)], although in other cases this mechanism might have to be complemented with (or substituted by) coherent detuned pumping [B. N. Nickolaus, D. Z. Zhang, and P. E. Toscheck, Phys. Rev. Lett. **47**, 171 (1981)]. However, this last contribution has not been modeled up to now [2,3].

[8] This could be achieved in practice with the configuration pointed out in Ref. [5] above.

[9] H. Haken, Phys. Lett. **53A**, 77 (1975).

[10] J. Guckenheimer and P. Holmes, *Nonlinear Oscillations, Dynamical Systems and Bifurcations in Vector Fields* (Springer-Verlag, Berlin, 1983).

[11] C. Z. Ning and H. Haken, Phys. Rev. A **41**, 6577 (1990).

[12] S. Newhouse, D. Ruelle, and F. Takens, Commun. Math. Phys. **64**, 35 (1978).

[13] P. W. Milonni, M. L. Shih, and J. R. Ackerhalt, *Chaos in Laser-Matter Interactions* (World Scientific, Singapore, 1987).